

Boundary massive sine-Gordon model at the free Fermi limit and RG flow of Casimir energy

Chaiho Rim

*Department of Physics, Chonbuk National University
Chonju 561-756, Korea
email: rim@chonbuk.ac.kr*

Abstract

RG flow of central charge c_{eff} is investigated for the two boundary sine-Gordon model at the free Fermi limit. Thermodynamic Bethe ansatz approach is used to check the non-monotonic decreasing properties of c_{eff} , its resonance, and the modification of c_{eff} due to the mismatch of the periodicity of a Lagrangian parameter and that of the boundary scattering parameter. The detailed analysis uses the singularity structure of the system on the complex rapidity plane.

1 Introduction

The c-theorem states that effective central charge c_{eff} decreases monotonically as the bulk system size increases [1]. This c-theorem is best studied and confirmed in the periodic bulk system of integrable field theories (IFT). IFT provides a non-perturbative study of the scale dependence of c_{eff} through thermodynamic Bethe ansatz (TBA) [2, 3]. TBA is a set of integral equations for spectral densities of the system, which uses the kernel derived from the scattering amplitude. c_{eff} is written in terms of the weighted integration of particle energy. It is remarkable that IR properties obtained from scattering matrices can be used to find the RG-flows from UV to IR. There are many examples which demonstrate the success of the TBA approach [4, 5, 6, 7, 8].

Notwithstanding the success, c_{eff} does not obey c-theorem always. In the presence of open boundaries non-monotonic behavior has been expected as well as resonances [9]. In addition, in some cases TBA does not fully reflect the UV properties of Lagrangian [10, 11, 12, 13]. This originates from the singularity structure of the system.

It is to be noted that even though the TBA equations are defined over the real rapidity variables, the physical rapidity space is not restricted to the real rapidity line. For a

periodic bulk system the rapidity is extended to complex values with $-\pi < \text{Im}(\theta) < \pi$. The singularity structure on the complex rapidity space provides all the information of particle spectra including bound states.

If the system has a boundary, then the physical rapidity plane reduces to $-\pi/2 < \text{Im}\theta < \pi/2$ and RG flow of c_{eff} can be seen in terms of R-channel TBA [14]. Depending on the boundary parameter ranges, the RG flow of c_{eff} is known to be much affected by the existence of singularities near the real rapidity axis. Especially, TBA may not have a finite solution at a certain parameter value, where singularities sit on the real rapidity. In this case, TBA is not well-defined beyond the parameter range and should be modified so that UV properties from the Lagrangian matches with IR properties from the scattering matrix. This demonstrates that complete understanding of the singularity structure is essential for understanding RG flow of c_{eff} .

In this paper, we study the singularity structure of the boundary sine-Gordon model (bsG) on a strip. bsG is given as [9]

$$\mathcal{A} = \int_0^R dx \int_{-\infty}^{\infty} \left\{ \frac{1}{4\pi} (\partial_a \varphi)^2 - 2\mu(\cos(2b\varphi) - 1) \right\} - 2\mu_B^{(L)} \int_{-\infty}^{\infty} dy \cos(b\phi_L - \chi_L) - 2\mu_B^{(R)} \int_{-\infty}^{\infty} dy \cos(b\phi_R - \chi_R).$$

where $\phi_L(y) = \varphi(0, y)$ ($\phi_R(y) = \varphi(R, y)$) is the boundary field living at the left (right) edge. R is the width of the strip representing the size of the system. The coupling constant b^2 is real and is restricted to be less than 1. (b^2 is scaled by 8π from the conventional choice $\beta^2 = 8\pi b^2$).

In fact, the integrability allows additional boundary terms,

$$-\frac{\alpha^{(L)}b}{\pi} \int_{-\infty}^{\infty} dy \frac{d\phi_L(y)}{dy} - \frac{\alpha^{(R)}b}{\pi} \int_{-\infty}^{\infty} dy \frac{d\phi_R(y)}{dy}.$$

Unlike in the one-boundary action, one cannot eliminate the whole term by introducing the bulk term [15],

$$-\frac{\alpha b}{\pi} \int_0^R dx \int_{-\infty}^{\infty} dy \partial_x \partial_y \varphi(x, y).$$

Therefore, the general action of bsG on a strip will be

$$\mathcal{A} = \int_0^R dx \int_{-\infty}^{\infty} \left\{ \frac{1}{4\pi} (\partial_a \varphi)^2 - 2\mu(\cos(2b\varphi) - 1) \right\} - \frac{\alpha b}{\pi} \int_{-\infty}^{\infty} dy \frac{d\phi_R(y)}{dy} - 2\mu_B^{(L)} \int_{-\infty}^{\infty} dy \cos(b\phi_L - \chi^{(L)}) - 2\mu_B^{(R)} \int_{-\infty}^{\infty} dy \cos(b\phi_R - \chi^{(R)}). \quad (1-1)$$

We will concentrate on the free fermionic limit of bsG, $b^2 = 1/2$ (or $\beta^2 = 4\pi$) [16]. This limit is chosen for simplicity and clarity since, even though (R-channel) TBA is known when the bulk scattering is diagonal, there appears a complicated singularity structure and imposes instability in the numerical analysis even in the massless case [12, 13].

The purpose of this paper is to understand RG-flow of c_{eff} and its dependence on the Lagrangian parameters through the singularity structure of the system. In section 2, we briefly summarize the relevant TBA analysis and analyze the domain of parameters. According to the boundary pole structure, the boundary parameters are classified into four Regimes: First, Lagrangian parameter χ is divided into two domains: $0 < \chi < \pi/2$ and its extended one $\pi/2 < \chi < \pi$. Then, each domain is divided according to the scattering parameter η appearing boundary scattering matrix in (2-5) below: $0 < \eta < \pi/2$ and $\pi/2 < \eta < \pi$. In section 3, massless limit of the theory is considered and the boundary parameter dependence of c_{eff} is summarized. Massless limit reduces the number of independent parameters and simplify the analysis a little bit. In section 4, massive theory with small boundary strength μ_B at both edges (called NN-type) is analyzed. In section 5, massive theory with large boundary strength μ_B at both edges (called DD-type) is analyzed. In section 6, the case with small μ_B at one edge and large μ_B the other edge (called ND-type) is analyzed. Section 7 is the conclusion. In Appendix Ising model is briefly presented.

2 Massive theory and boundary conditions

The TBA of the free Fermi limit is simply given as

$$\epsilon_0 = 2r \cosh \theta \quad (2-1)$$

with $M = 2\pi\mu$ and $r = MR$. This does not mean that the system is trivial. All the essential difficulties lies in the non-trivial boundary action, which induces complex singularity structures. The effective central charge is given as

$$c_{\text{eff}} = \frac{6r}{\pi^2} \int_{-\infty}^{\infty} d\theta \cosh \theta \log Z(\theta) \equiv c - 24\Delta, \quad (2-2)$$

where

$$Z(\theta) = 1 + \lambda_0(\theta) e^{-\epsilon_0} + \lambda_d(\theta) e^{-2\epsilon_0}. \quad (2-3)$$

Here λ_0 and λ_d are fugacity due to the boundary effect, compactly written as [11]

$$\begin{aligned} \lambda_0(\theta) &= \overline{K_L^{++} K_R^{++}} + \overline{K_L^{+-} K_R^{+-}} + \overline{K_L^{-+} K_R^{-+}} + \overline{K_L^{--} K_R^{--}} = \text{Tr}(\overline{K_L} K_R) \\ \lambda_d(\theta) &= (\overline{K_L^{++} K_L^{--}} - \overline{K_L^{+-} K_L^{-+}})(K_R^{++} K_R^{--} - K_R^{+-} K_R^{-+}) = \text{Det}(\overline{K_L} K_R), \end{aligned}$$

where the overlines denote for complex conjugate operation. Subscript L and R stand for the left and right edge contribution. $K_{L,R}$ is obtained from the boundary scattering amplitude $R_{L,R}(\theta)$, $K(\theta) = R(i\frac{\pi}{2} - \theta)$. Explicitly they are written in terms of soliton and anti-soliton basis [9],

$$K^{\xi\xi}(\eta, \vartheta|\theta) = P^{\xi}(\eta, \vartheta|\theta) G(\eta, \vartheta|\theta), \quad K^{\xi,-\xi}(\eta, \vartheta|\theta) = Q^{\xi}(\eta, \vartheta|\theta) G(\eta, \vartheta|\theta) \quad (2-4)$$

where $\xi = \pm$ and

$$P^{\xi}(\eta, \vartheta|\theta) = -i \sinh(\theta) \cos(\eta) \cosh(\vartheta) - \xi \cosh(\theta) \sin(\eta) \sinh(\vartheta)$$

$$\begin{aligned}
Q^\xi(\alpha|\theta) &= ie^{-\xi 2i\alpha} \sinh(\theta) \cosh(\theta) \\
G(\eta, \vartheta|\theta) &= \frac{1}{\left(2 \cos\left(\frac{\eta+i\theta}{2}\right) \cos\left(\frac{\eta-i\theta}{2}\right)\right) \left(2 \cosh\left(\frac{\vartheta+\theta}{2}\right) \cosh\left(\frac{\vartheta-\theta}{2}\right)\right)}.
\end{aligned} \tag{2-5}$$

After some manipulation, λ_d and λ_0 are written as

$$\begin{aligned}
\lambda_d &= \tan\left(\frac{\eta_L - i\theta}{2}\right) \tan\left(\frac{\eta_L + i\theta}{2}\right) \tanh\left(\frac{\vartheta_L - \theta}{2}\right) \tanh\left(\frac{\vartheta_L + \theta}{2}\right) \\
&\quad \tan\left(\frac{\eta_R - i\theta}{2}\right) \tan\left(\frac{\eta_R + i\theta}{2}\right) \tanh\left(\frac{\vartheta_R - \theta}{2}\right) \tanh\left(\frac{\vartheta_R + \theta}{2}\right)
\end{aligned} \tag{2-6}$$

$$\begin{aligned}
\lambda_0 &= 2 \left(\sinh^2 \theta \cos \eta_L \cos \eta_R \cosh \vartheta_L \cosh \vartheta_R + \cosh^2 \theta \sin \eta_L \sin \eta_R \sinh \vartheta_L \sinh \vartheta_R \right. \\
&\quad \left. + \cosh^2 \theta \sinh^2 \theta \cos(2\alpha) \right) G_L(\eta, \vartheta, \tilde{u}) G_R(\eta, \vartheta, \tilde{u}).
\end{aligned} \tag{2-7}$$

From the fugacity one can check the periodic property of Z in (2-3),

$$Z(\theta + i2\pi) = Z(\theta), \quad Z(\theta + i\pi) = Z(\theta) e^{2\epsilon_0(\theta)} / \lambda_0(\theta). \tag{2-8}$$

$K^{\xi, -\xi}$ in (2-4) represents the soliton number violation scattering at the edge and contains the parameter α which is identified with the Lagrangian parameter α in (1-1). This is because the boundary derivative term in (1-1) shifts the conjugate momentum of the field $\Pi = \dot{\phi}/(2\pi)$ by $-\alpha\delta(x-R)/\pi$, and as the consequence, the phase of the soliton operator in [17] is shifted by α , $e^{i\alpha}$.

The scattering parameters η and ϑ are related to the Lagrangian parameters $m_B \equiv \mu_B \sqrt{2\pi/M}$ and $0 < \chi < \pi$ [18]:

$$\cos(\eta/2) \cosh(\vartheta/2) = m_B \cos \chi, \quad \sin(\eta/2) \sinh(\vartheta/2) = m_B \sin \chi. \tag{2-9}$$

η has the mirror symmetry with respect to $\chi = \pi/2$, $\eta(\chi) = \eta(\pi - \chi)$, whose explicit relation is plotted in Figure 1.

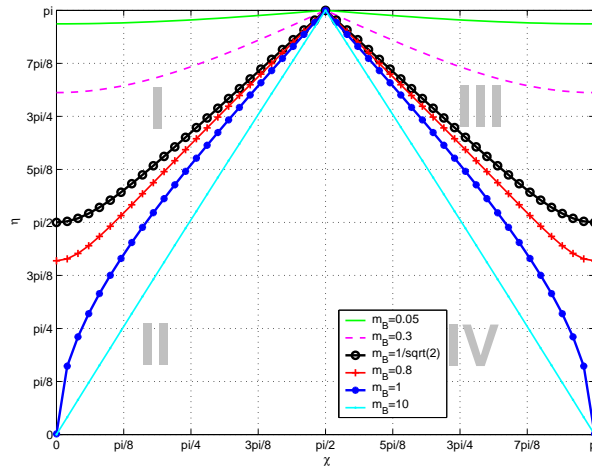


Figure 1: η v.s. χ

Note that the boundary bound state spectrum is [9, 20]

$$\mathcal{E}_B = M \cos \nu, \quad \nu = \eta - \pi/2 \quad \text{or} \quad \pi - (\eta - \pi/2) \tag{2-10}$$

where $0 < \nu < \pi/2$. Thus, if $0 < \eta < \pi/2$ there is no boundary bound state. According to the existence of a boundary bound state, we conveniently classify the boundary parameters into four Regimes:

$$\begin{array}{ll}
\text{Case } 0 < \chi < \pi/2 : & \begin{array}{ll} \text{when } \pi/2 < \eta < \pi & \text{Regime I} \\ \text{when } 0 < \eta < \pi/2 & \text{Regime II} \end{array} \\
\text{Case } \pi/2 < \chi < \pi : & \begin{array}{ll} \text{when } \pi/2 < \eta < \pi & \text{Regime III} \\ \text{when } 0 < \eta < \pi/2 & \text{Regime IV.} \end{array}
\end{array}$$

It is convenient to define χ_c which satisfies $\eta(\chi_c) = \pi/2$. χ_c is restricted to the value $0 \leq \chi_c \leq \pi/2$. When $0 < m_B < 1/\sqrt{2}$ (which will be called N-type boundary condition), $\chi_c = 0$ and only Regimes I and III are allowed. On the other hand, when $1/\sqrt{2} < m_B$ (called D-type boundary condition), $0 < \chi_c < \pi/4$ and all of the four Regimes are allowed.

One may wonder if Regime I and III (II and IV) are the same each other. However, this is not the case. The reason is that scattering data and Lagrangian data do not coincide each other in Regime I and III (II and IV) : The periodicity of $\eta_{L/R}$ in the scattering amplitude differs from that in the Lagrangian. $\eta_{L/R}$ in (2-5) is periodic in π and the symmetry $\chi \rightarrow -\chi$ restricts the domain of χ as

$$0 < \chi < \pi/2 \quad \text{in TBA.} \quad (2-11)$$

On the other hand, χ in Lagrangian (1-1) is periodic in 2π and is restricted to

$$0 < \chi < \pi \quad \text{in Lagrangian.} \quad (2-12)$$

The periodicity of χ from the scattering data does not match with the one given from the Lagrangian. This suggests that c_{eff} obtained from TBA approach (3-3) is in trouble when $\chi > \pi/2$ (Regime III and IV) since TBA uses the IR scattering data.

One would simply double the period of χ in (2-5). But this does not solve the problem. Suppose one extends the zone of χ of one edge to $0 < \chi < \pi$. Then, $c_{\text{eff}}(\chi) = c_{\text{eff}}(\pi - \chi)$. On the other hand, replacing χ into $\pi - \chi$ in the action will change the sign of the boundary term since μ_B will be replaced with $-\mu_B$. This means that c_{eff} is insensitive to the sign of the boundary action and will have a cusp at $\chi = \pi/2$, which is not sound from the physics point of view [11]. Thus c_{eff} given in (3-3) has to be modified in the extended parameter space. This possibilities are to be treated in detail in next sections.

The parameter α has no periodicity problem: α in (2-5) is periodic in π . On the other hand, α -term in the action (1-1) will give an exponential factor in the partition function $e^{-2i\alpha(\frac{b\Delta\phi_0}{2\pi})}$. Since $b\Delta\phi_0/(2\pi)$ is an integer (winding number), the periodicity of α is π , same as in the scattering data. Thus, the range of α may be reduced to the domain $-\pi/2 < \alpha < \pi/2$. Using the symmetry $\alpha \rightarrow -\alpha$ in λ_0 , the domain can be further reduced to

$$0 < \alpha < \pi/2. \quad (2-13)$$

3 Massless limit

The effect of the boundary parameters on c_{eff} is easier to understand if the number of parameters can be reduced. The massless theory is a good example of this. In this section, we summarize the singularity structure at the massless limit of bSG.

The massless limit is obtained by rescaling the parameters appropriately [19]. Introducing a large rapidity parameter θ_0 , one rescales the mass scale $(M/2)e^{\theta_0} \rightarrow M$, rapidity $\theta \rightarrow \theta + \theta_0$, and boundary parameter $\vartheta \rightarrow \vartheta + \theta_0$. Therefore, one has the parameter relation,

$$e^{\vartheta} = 4\pi\mu_B^2/M, \quad \eta = 2\chi. \quad (3-1)$$

The rescaled quantities simplify the scattering data of (2-4) :

$$K^{\xi\xi}(u) = -i e^{-\xi i\eta} \frac{e^{\frac{1}{2}(\vartheta-\theta)}}{2 \cosh\left(\frac{\vartheta-\theta}{2}\right)}, \quad K^{\xi,-\xi}(u) = i e^{-\xi 2i\alpha} \frac{e^{-\frac{1}{2}(\vartheta-\theta)}}{2 \cosh\left(\frac{\vartheta-\theta}{2}\right)}. \quad (3-2)$$

The effective central charge is written as

$$c_{\text{eff}} = \frac{12r}{\pi^2} \int_{-\infty}^{\infty} d\theta e^{\theta} \log Z(\theta) \quad (3-3)$$

where $Z(\theta)$ is the massless limit of (2-3) with $\epsilon_0 = 2re^{\theta}$ and

$$\begin{aligned} \lambda_0 &= \frac{\cos \eta e^{(\frac{\vartheta_L + \vartheta_R}{2} - \theta)} + \cos(2\alpha) e^{-(\frac{\vartheta_L + \vartheta_R}{2} - \theta)}}{2 \cosh\left(\frac{\vartheta_L - \theta}{2}\right) \cosh\left(\frac{\vartheta_R - \theta}{2}\right)} \\ \lambda_d &= \tanh\left(\frac{\vartheta_L - \theta}{2}\right) \tanh\left(\frac{\vartheta_R - \theta}{2}\right). \end{aligned} \quad (3-4)$$

In this massless limit, only the combination of χ_L and χ_R enters in c_{eff} with $\eta = 2\chi = 2(\chi_R - \chi_L)$ and boundary bound state disappears in (3-2). This simplifies the analysis greatly.

The fugacity is written in a simple form when both of the boundaries are given in an extreme condition so that they can be treated as a conformal field theory (CFT). When both edges are in Dirichlet limit ($\vartheta_L = \vartheta_R \rightarrow \infty$) or in Neumann limit ($\vartheta_L = \vartheta_R \rightarrow -\infty$): $\lambda_0 = 2 \cos \zeta$ and $\lambda_d = 1$ with $\zeta = 2\chi$ for Dirichlet and $\zeta = 2\alpha$ for Neumann condition. In this limit

$$c_{\text{eff}} = 1 - 3\zeta^2/\pi^2, \quad (3-5)$$

where $-\pi < \zeta < \pi$. This result is obtained using the integration result for

$$\int_0^{\infty} ds \log(1 + 2 \cos \zeta e^{-s} + e^{-2s}) = \frac{\pi^2}{6} - \frac{\zeta^2}{2}.$$

The conformal dimension of the ground state is given as $\Delta = \zeta^2/(8\pi^2)$, which reflects the duality between the role of α of Neumann condition and the role of χ of Dirichlet condition in CFT of a compact boson theory.

When one edge is given in Neumann limit and the other edge in Dirichlet limit, $\lambda_0 = 0$ and $\lambda_d = -1$. Then the effective central charge is independent of χ and α ,

$$c_{\text{eff}} = -\frac{1}{2}, \quad (3-6)$$

since

$$\int_0^\infty ds \log(1 - e^{-2s}) = -\frac{\pi^2}{12}.$$

The conformal dimension of the ground state is given as $\Delta = 1/16$.

The effect of α on c_{eff} is plotted in figure 2 at $\chi = 0$. The dependence of c_{eff} on α is manifest when both boundaries are given as Neumann condition; the smaller ϑ is, the greater the effect.

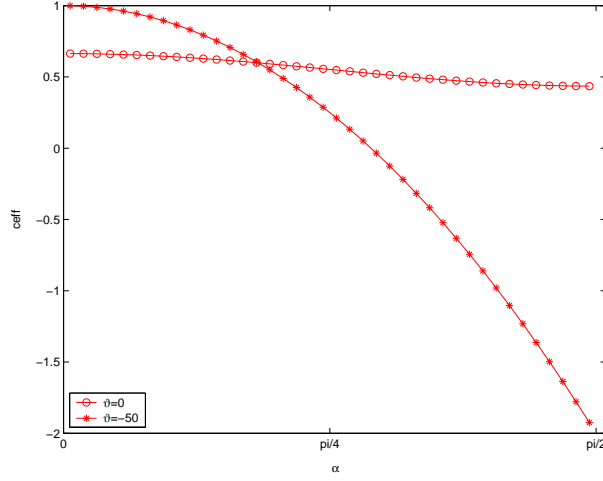


Figure 2: c_{eff} v.s. α at $\chi_L = \chi_R = 0$.

The figure 2 implies that when plotting c_{eff} v.s. ϑ with fixed α and χ there will appear a bump at a sufficiently large α . The bump is the result of the interference between the ground state and an excited state. This will be discussed in detail in section 4.

On the other hand, the branch-cut singularities arise in c_{eff} when

$$Z(\theta) = 0. \quad (3-7)$$

This type of singularity will be called Z_0 -singularity (Z_0S). There are infinite number of Z_0S 's and all of them lie at $\text{Im}(\theta) = \pm\pi/2$. When $\eta = \pi$ ($\chi = \pi/2$) and $\alpha = 0$, however, there appears Z_0S at the real rapidity axis since

$$Z(\theta) = \left(1 - \tanh\left(\frac{\vartheta_L - \theta}{2}\right)\right) \left(1 - \tanh\left(\frac{\vartheta_R - \theta}{2}\right)\right).$$

This is the source of trouble for the mismatch of the period of χ in two approaches, TBA and Lagrangian. One cannot simply extend the domain of $\chi < \pi/2$ to $\chi > \pi/2$ but has to take care of the singularity at $\chi = \pi/2$ properly [10, 11, 12, 13].

One way to proceed is to analytically continue $\chi < \pi/2$ by complexifying η and rotating around at π so that one can arrive at other domain of $\chi > \pi/2$. Under this operation, one notices that for the ground state a singularity at $i\pi/2 + \theta_p$ (θ_p is real and positive crosses the real rapidity line and sits at $-i\pi/2 + \theta_p$ (or vice versa) [12]. This singularity will be called Z_0 -crossing singularity (Z_0CS).

Z_0CS pushes the integration contour around the cross singularity position so that c_{eff} is put as

$$c_{\text{eff}} = -\frac{24r}{\pi} e^{\theta_p} + \frac{12r}{\pi^2} \oint_{-\infty}^{\infty} d\theta e^{\theta} \log Z(\theta). \quad (3-8)$$

The first term in RHS is due to the singularity crossing and the second one is the real axis contribution where \oint represents the principal value of the integration.

Figure 3 is the plot obtained from (3-3) when $\chi < \pi/2$, and (3-8) when $\chi > \pi/2$. In this modified version, the curve is not cusped at $\chi = \pi/2$, but is smooth and the period of c_{eff} matches with the period of Lagrangian.

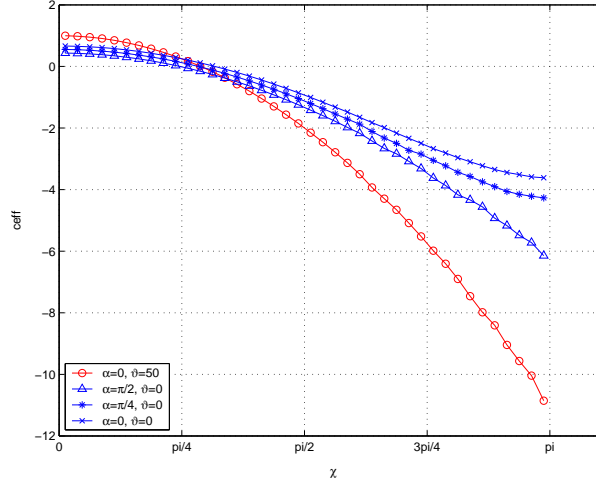


Figure 3: c_{eff} v.s. χ for $0 < \chi < \pi$ from the modified c_{eff} .

4 NN-type boundary condition

In this section, the boundary strength m_B of both edges are considered to be small, $m_B^{(L,R)} < 1/\sqrt{2}$ (called NN-type). In this case the boundary bound state exists and Regime I and III ($\pi/2 < \eta < \pi$) are allowed.

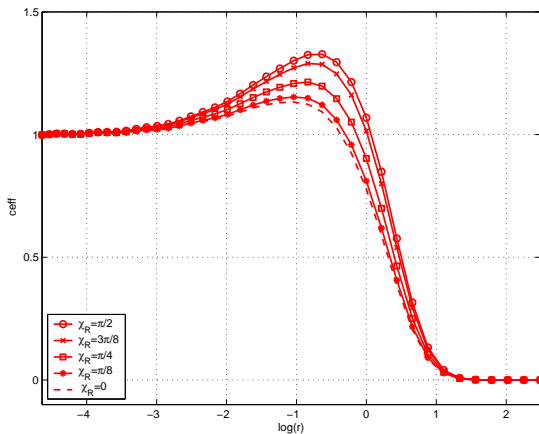


Figure 4: c_{eff} v.s. $\log(r)$ at $m_B^{(L)} = m_B^{(R)} = 0.2$ and $\chi_L = \alpha = 0$.

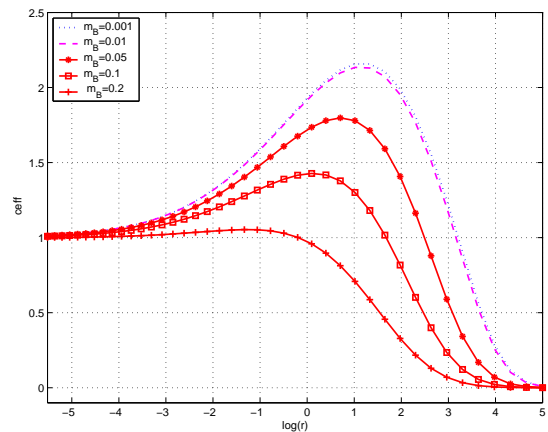


Figure 5: c_{eff} v.s. $\log(r)$ at $\chi_R = \chi_L = 0$ and $\alpha = 0$. Here $m_B = m_B^{(L)} = m_B^{(R)}$.

In figure 4, c_{eff} is plotted against $\log(r)$ for Regime I when $\alpha = 0$. In UV limit ($r \rightarrow 0$), $c_{\text{eff}} \rightarrow 1$ and is independent of χ . This limit corresponds to the Neumann limit of the massless theory. In IR limit ($r \gg 1$), $c_{\text{eff}} \rightarrow 0$. In between UV and IR, c_{eff} is not monotonically decreasing but there appears a resonance bump. This resonant bump is enhanced as $m_B^{(L/R)}$ approaches 0, which is seen in figure 5.

The resonance implies that the ground state interferes with the excited state, the boundary bound state. This is explained from the singularity structure. Note that a boundary bound state provides a pair of poles in Z (2-3), which will be called Z_∞ singularity ($Z_\infty S$),

$$Z = \infty. \quad (4-1)$$

$Z_\infty S$ lies at $\pm i(\pi - \eta)$ with $0 < (\pi - \eta) < \pi/2$. This is shown in figure 6.

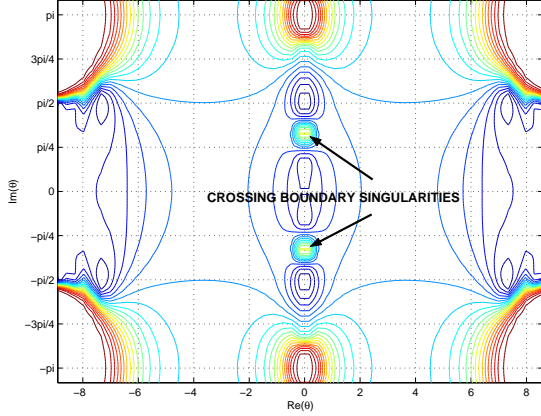


Figure 6: Contour plot of Z_∞ singularities. Crossing singularities lie at the imaginary axis in the physical strip.

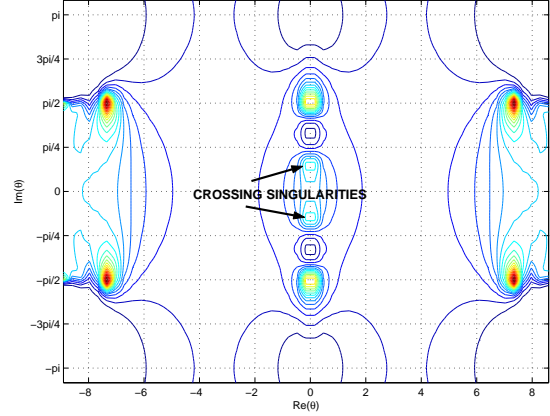


Figure 7: Contour plot of Z_0 singularities. Crossing singularities are squeezed between Z_∞ crossing singularities.

Most of $Z_0 S$'s lie at $\pm(i\pi/2 \pm \theta_D)$, where $\theta_D > 0$ is real and depends on the scale as well as the boundary parameters. At $\theta_D = 0$, there is a ubiquitous singularity pair. In addition to this, an additional pair exists at $\pm i\theta_N$ in this NN-type boundary condition where $0 < \theta_N < (\pi - \eta)$. As $r \gg 1$, $\theta_N \rightarrow (\pi - \eta)$. The singularities are given in figure 7.

In this NN-type, the ground state with m_B can be degenerate with the ground state with $-m_B$ as $r \rightarrow \infty$ and $m_B \rightarrow 0$. In the intermediate scale, the two states are not completely degenerate but interfere with each other. This is because as $\chi \rightarrow \pi/2$ or $m_B \rightarrow 0$, $\eta \rightarrow \pi$ and $Z_\infty CS$ at $\pm i(\pi - \eta)$ moves close to the real rapidity line. At the same time $Z_0 CS$ squeezed between this $Z_\infty CS$ moves close to the real line too. In fact, $Z_\infty S$ at $\pm i(\pi - \eta)$ and $Z_0 S$ at $\pm i\theta_N$ are crossing and the ground state with $-\mu_B$ can be obtained from the ground state with μ_B by taking care of the crossing singularity. (See Eq. (4-2) below). As the singularities lie near the real rapidity axis the two states interfere each other strongly. This resonance effect is first noticed in Ising system in the presence of weak magnetic field in [9]. (See Appendix for Ising model).

In Regime III ($\chi > \pi/2$), one has to count in crossing singularities, which cure c_{eff} to have the right periodicity of χ . When $\chi = \pi/2$, $\eta = \pi$ and the singularity sits at $\theta = 0$. Thus $\chi = \pi/2$ is the singular point in the parametric space. One may analytically

continue χ into the extended domain $\pi/2 < \chi < \pi$. (Equivalently, one may analytically continue m_B around $m_B = 0$. See this possibility in boundary Lee-Yang case [10])

Under the analytic continuation, $Z_\infty CS$ as well as $Z_0 CS$ is crossing at the same time. The ground state contribution is obtained by minimizing the number of crossing singularities and taking the crossing singularities close to the imaginary axis.

In figure 6 and 7, the the crossing singularities are pointed with arrows. $Z_\infty CS$ is given as $\pm i(\pi - \eta_R)$ and $Z_0 CS$ as $\pm i\theta_N$. When only one edge's χ exceeds $\pi/2$, c_{eff} is modified as

$$c_{\text{eff}} = -\frac{24r}{\pi} \left(\sin \theta_N - \sin \eta_R \right) + \frac{6r}{\pi^2} \int_{-\infty}^{\infty} d\theta e^{\theta} \log Z(\theta), \quad (4-2)$$

where the right edge is chosen to have $\chi_R > \pi/2$. θ_N is the real function of r , m_B , χ , and α . Even though the exact dependence of θ_N is not known analytically, it can be calculated numerically. When $r \rightarrow \infty$, $\theta_N \rightarrow \eta_R$. When $r \rightarrow 0$, $\theta_N \rightarrow \theta_0$ and θ_0 vanishes as $m_B \rightarrow 0$. At UV limit, $c_{\text{eff}} = 1$ and at IR limit, $c_{\text{eff}} = 0$. In figure 8, plotted is c_{eff} v.s. $\log(r)$ when $m_B^{(L/R)} = 0.2$, and $\alpha = \chi_L = 0$.

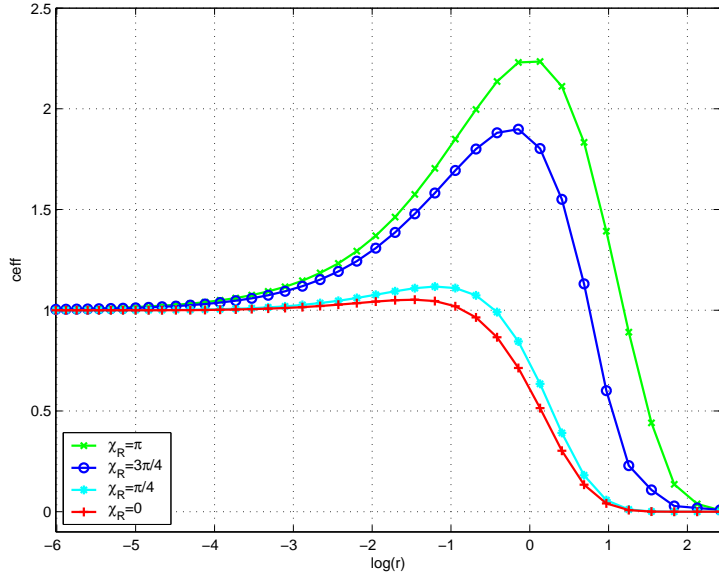


Figure 8: c_{eff} v.s. $\log(r)$ at $m_B^{(L)} = m_B^{(R)} = 0.2$ and $\alpha = \chi_L = 0$. Curves with $\chi_R = 0, \pi/4$ belong to Regime I, and $\chi_R = 3\pi/4, \pi$ to Regime III.

In figure 8 $m_B^{(L)} = m_B^{(R)}$ is used. When $m_B^{(L)} \neq m_B^{(R)}$ one needs to calculate c_{eff} in two ways and chooses the minimum as the ground state result among the two : One with (χ_L, χ_R) and the other with $(\widetilde{\chi}_L, \widetilde{\chi}_R)$ where $\widetilde{\chi}_L = \pi - \chi_L$ and $\widetilde{\chi}_R = \pi - \chi_R$. This is because bsG with (χ_L, χ_R) is equivalent to one with $(\widetilde{\chi}_L, \widetilde{\chi}_R)$ under the field operation, $b\varphi \rightarrow b\varphi + \pi$ and $(\varphi \rightarrow -\varphi)$, but the crossing singularity contribution can be different.

Suppose both χ 's exceed $\pi/2$, (e.g., $\chi_L > \pi/2$ and $\chi_R > \pi/2$). Then one may rearrange both parameters as $\widetilde{\chi} < \pi/2$ so that the crossing singularities do not contribute. If one would count in the crossing singularities of both edges, then c_{eff} would be of an excited state result rather than of the ground state one.

The parameter α also affects c_{eff} . Especially, at UV limit the effect is manifest and $c_{\text{eff}} \neq 1$ when $\alpha \neq 0$. One may convince oneself that at UV limit c_{eff} v.s. α reproduces the CFT limit (3-5). This behavior is plotted in figure 9. (Refer to figure 14 below also).

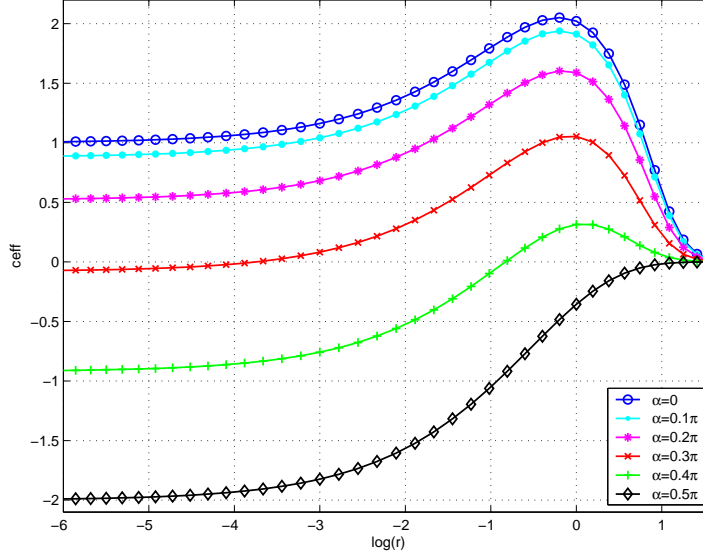


Figure 9: c_{eff} v.s. $\log(r)$ at $\chi_R = \chi_L = 0$ and $m_B = 0.001$ with various α .

At IR limit, however, α effect vanishes and $c_{\text{eff}} \rightarrow 0$. Therefore, RG-flow between UV and IR is not monotonically decreasing. A resonance bump is also seen at the intermediate scale due to the singularities near the real axis.

5 DD-type boundary condition

In this section, both edges are restricted to DD-type ($m_B^{(L/R)} > 1/\sqrt{2}$). In DD-type, all the four Regimes are to be considered. To simplify the analysis, we put $m_B = m_B^{(L)} = m_B^{(R)}$.

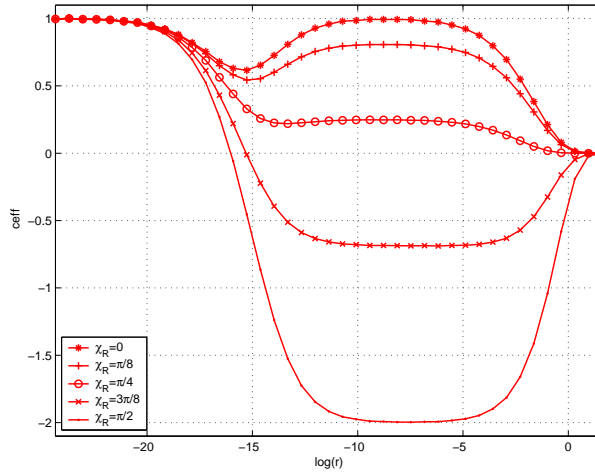


Figure 10: c_{eff} v.s. $\log(r)$: $m_B^{(L)} = m_B^{(R)} = 1000$ and $\chi_L = \alpha = 0$.

At IR limit $c_{\text{eff}} \rightarrow 0$. At UV limit $c_{\text{eff}} \rightarrow 1$ when $\alpha = 0$. However, at the intermediate scale, the plot c_{eff} v.s. r (or c_{eff} v.s. $\log(r)$) shows a new feature. In figure 10, c_{eff} v.s. $\log(r)$ is plotted for $m_B = 1000$ and $\alpha = 0$. (Here $\chi_R = 0, \pi/8$ belong to Regime II, and $\chi_R = 3\pi/8, \pi/2$ to Regime I.) There appears a plateau around $\log(r) \approx -8$ (here $\vartheta \approx 15 \gg 1$), which corresponds to the massless limit : c_{eff} v.s. χ at this plateau reproduces the value in the massless limit figure 3. The plateau appears around $-\log(r/2) \approx \vartheta/2 \gg 1$, which is between $-\log(r/2) \approx \vartheta$ and $-\log(r/2) \approx 1$. The bigger m_B , the wider the plateau becomes. This is why the massless limit is easily obtained when $m_B \gg 1$. The Dirichlet limit of the massless theory corresponds to the extreme limit $m_B \rightarrow \infty$.

Note that the massless limit does not coincide with the UV limit. For a sufficiently large $m_B \gg 1$, ϑ provides a large characteristic energy scale. One may rescale the rapidity around ϑ to see the massless limit, which is considered in Sec. 3. UV limit appears when the energy scale is greater than ϑ (length scale is smaller than $-\log(r/2) \approx \vartheta$).

In regime I ($\chi_c < \chi < \pi/2$), the boundary bound state exists. Thus Z_∞ has the singularity in the physical strip at $\pm i(\pi - \eta_{L/R})$. In figure 11, $Z_\infty S$ is shown when $\alpha = 0$, $m_B = 1000$, $\chi_L = 0$, $\chi_R = 2\pi/5$ and $\log(r) \approx -10$. (Here $\eta_R = 4\pi/5$ and $\eta_L = 0$).

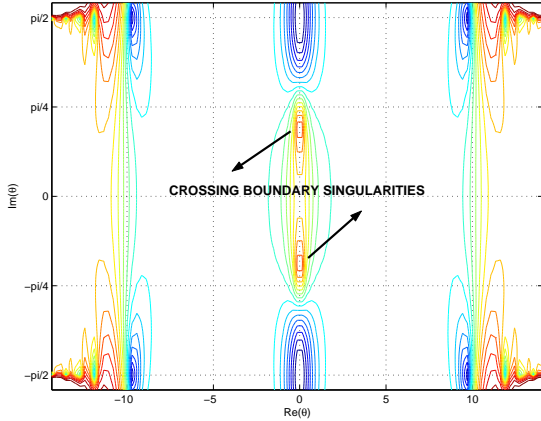


Figure 11: Contour plot of $Z_\infty S$. $Z_\infty CS$ is identified with arrows.

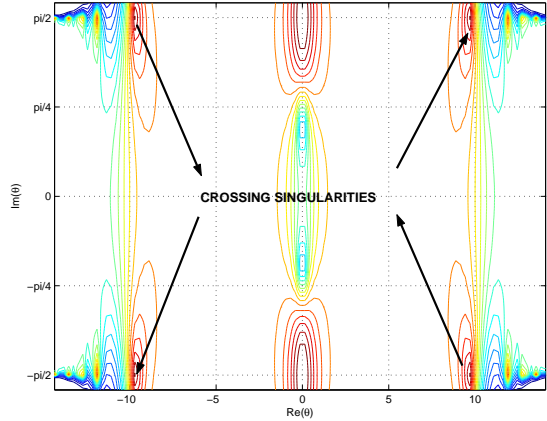


Figure 12: Contour plot of $Z_0 S$. $Z_0 CS$ is identified with arrows.

$Z_0 S$ lies at $\text{Im}(\theta) = \pm\pi/2$ as $r \ll 1$. The singularities accumulate around at $\theta = \pm(i\pi/2 \pm \log(r/2))$ along with the isolated one at $\theta = \pm i\pi/2$ as shown in figure 12. However, as $r \gg 1$, a pair of (crossing) singularities appear at the pure imaginary rapidity axis $\pm i\theta_N$ with θ_N real, $(\pi - \eta) < \theta_N < \pi/2$.

Regime III ($\pi/2 < \chi < (\pi - \chi_c)$) is the analytically continuation of Regime I and c_{eff} is modified according to the crossing singularities. Suppose $\chi_L = 0$ and $\pi/2 < \chi_R < (\pi - \chi_c)$. We need to consider two cases separately, r large and r small. When $Z_0 CS$ is given as $\pm(\theta_D \pm i\pi/2)$ (the case when r is small),

$$c_{\text{eff}} = -\frac{24r}{\pi} \left(\cosh \theta_D - \sin \eta_R \right) + \frac{6r}{\pi^2} \int_{-\infty}^{\infty} d\theta e^{\theta} \log Z(\theta). \quad (5-1)$$

When Z_0 crossing singularity is given as $\pm i\theta_N$ (the case when r is large),

$$c_{\text{eff}}(\chi) = -\frac{24r}{\pi} \left(\sin \theta_N - \sin \eta_R \right) + \frac{6r}{\pi^2} \int_{-\infty}^{\infty} d\theta e^{\theta} \log Z(\theta). \quad (5-2)$$

In UV limit, (5-1) gives $c_{\text{eff}} \rightarrow 1$. In IR limit, as $\theta_N \rightarrow \pi - \eta_R$ (5-2), $c_{\text{eff}} \rightarrow 0$. This behavior is seen in figure 13 when $\chi_R = 3\pi/5$.

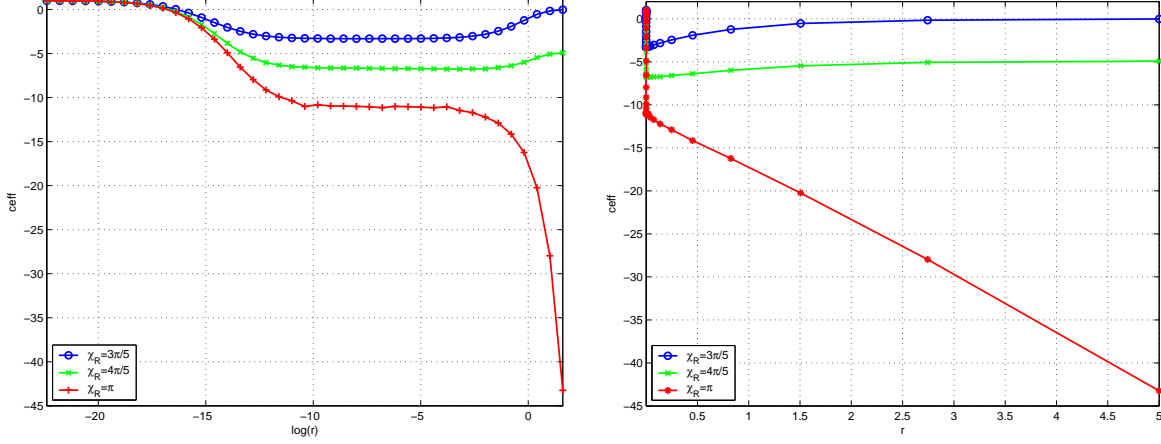


Figure 13: c_{eff} v.s. $\log r$ (left) and c_{eff} v.s. r (right) with $m_B^{(L)} = m_B^{(R)} = 1000$. $\chi_R = 3\pi/5$ is in Regime III and $\chi_R = 4\pi/5, \pi$ are in Regime IV.

In Regime II, ($0 < \chi < (\pi - \chi_c)$), there is no boundary bound states and therefore no $Z_\infty S$ on the physical strip. $Z_0 S$ is given as $\text{Im}(\theta) = \pi/2$. Analytically continuing to Regime IV ($(\pi - \chi_c) < \chi < \pi$), one has $Z_0 C S$ at $\pm(\theta_D \pm i\pi/2)$ with θ_D real and positive. It is noted however, even though there is no boundary bound states, $Z_\infty C S$ is at $\pm i(\pi - \eta_R)$, which is outside of physical strip. Thus, c_{eff} is given as the same form of (5-1):

$$c_{\text{eff}} = -\frac{24r}{\pi} \left(\cosh \theta_D - \sin \eta_R \right) + \frac{6r}{\pi^2} \int_{-\infty}^{\infty} d\theta e^{\theta} \log Z(\theta). \quad (5-3)$$

The r -dependence is given in figure 13 for $\chi_R = 4\pi/5$ and π . In the intermediated scale, the plateau reproduces the massless limit in figure 3. As $r \gg 1$, one sees that c_{eff} has the tendency of decreasing linearly in r . In fact, $\theta_D \rightarrow 0$ at IR limit and as a result

$$c_{\text{eff}}(\chi) = -\frac{24r}{\pi} (1 - \sin \eta_R) + O(e^{-2r}). \quad (5-4)$$

The linearity of c_{eff} in r indicates that if one changes the sign of one edge, the free energy density $f(r)$ in IR limit becomes bigger than the case with the same sign:

$$\Delta f = -\frac{\pi}{24R} \Delta c_{\text{eff}} = M - M \sin \eta_R. \quad (5-5)$$

The additional free energy corresponds to the one soliton mass M compensated by the right edge boundary excitation energy $M \sin \eta_R$. Thus, one may subtract this IR amount from c_{eff} and equivalently, re-normalize the free energy density.

Finally, α effect is vanishingly small at IR limit. However, the α effect is enhanced at r smaller than the plateau region. Especially, at UV limit c_{eff} is not 1 but depends on values of α . c_{eff} v.s. α at UV limit reproduces the CFT limit, which is plotted in figure 14.

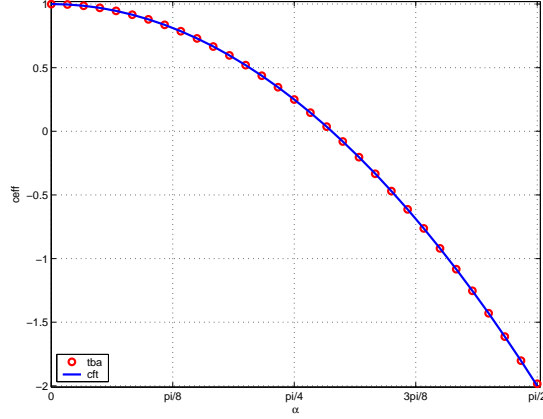


Figure 14: c_{eff} v.s. α : $r = \exp(-23)$ and $m_B = 100$.

6 ND-type boundary condition

In this section, we will give a few comments when combination of N-type at one edge and D-type at the other edge is given. Suppose the boundary strength at the left edge is neglectingly small ($m_B^{(L)} \sim 0$) and that of the right edge is large ($m_B^{(R)} \gg 1/\sqrt{2}$). In this case the singularity crossing effect can be neglected. (Note that one may choose $\chi < \pi/2$ if $m_B^{(L)} = 0$ using the action symmetry). Still, there remains a plateau, corresponding to the massless limit in addition to the UV limit.

At UV, one sees the enhanced role of the compact boson property, $c_{\text{eff}} \rightarrow 1 - 12(\alpha/\pi)^2$, independent of χ . At the plateau, one may confirm that c_{eff} is independent of χ and α and approaches to $-1/2$. This results in $\Delta = 1/16$, the dimension of the ground state. One may see this behavior in figure 15.

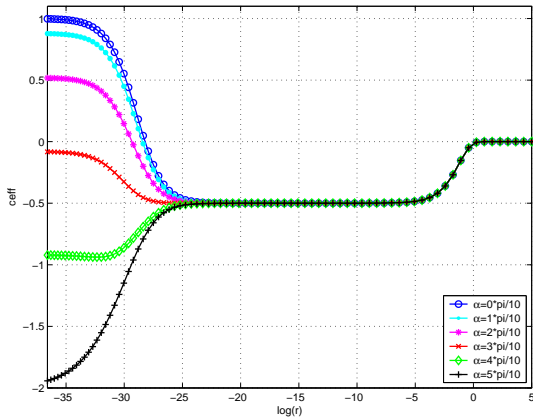


Figure 15: c_{eff} v.s. $\log(r)$ with various α : $m_B^{(L/R)} = (10^{-2}, 10^6)$ and $\chi_{L/R} = (0, \pi/4)$.

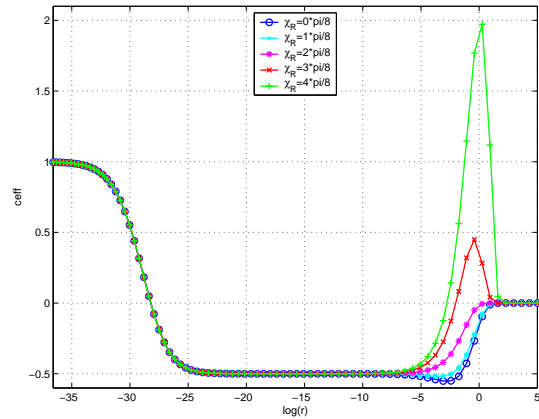


Figure 16: c_{eff} v.s. $\log(r)$ with various χ : $m_B^{(L/R)} = (10^{-2}, 10^6)$ and $\alpha = 0$.

At IR $c_{\text{eff}} \rightarrow 0$. In addition, as $r \gg 1$, there appears a resonance bump. The resonance behavior is more enhanced as $\chi_R \rightarrow \pi/2$, since the singularities move close to the real rapidity axis. This is clearly seen in figure 16.

If the boundary strength m_B is not in the extreme case, the singularity crossing contribution is not significant. When one edge is in $0 < \chi < \pi/2$ and the other edge in $\pi/2 < \chi < \pi$, using the action symmetry one may re-arrange the N-type boundary in $\pi/2 < \chi < \pi$ (Regime III) and D-type boundary in $0 < \chi < \pi/2$ (Regime II) so that one counts in the singularity crossing from the N-type boundary, which will give the ground state contribution.

7 Conclusion

To summarize, we consider the free fermion limit of the massive boundary sine Gorodn model on a strip and investigate the boundary parameter effect on the RG flow of c_{eff} . For a certain range of parameters, the flow shows $c_{\text{eff}} = 0$ at IR limit, and $c_{\text{eff}} \rightarrow 1 - 12(\alpha/\pi)^2$ at UV limit. However, depending on the parameter ranges the RG flow is not monotonic and shows much more diverse effects at the intermediate scale. All the anomalous behavior originates from the singularity structure on the complex rapidity space.

In NN-type boundary condition ($m_B^{(L/R)} < 1\sqrt{2}$), UV limit and massless limit coincide. In the intermediate scale a resonance appears due to the singularity close to the real rapidity axis. If one edge is in $0 < \chi < \pi/2$ (Regime I), and the other edge is in $\pi/2 < \chi < \pi$ (Regime III), then the singularity crossing is to be counted to modify the c_{eff} formula.

In DD-type boundary condition ($m_B^{(L/R)} > 1\sqrt{2}$), UV limit does not coincide with the massless limit. The massless limit appears as the plateau in c_{eff} v.s. $\log(r)$, which is characterized by the scale $r \sim e^{-\vartheta}$. The Dirichlet limit of this plateau reproduces the massless result, $c_{\text{eff}} \rightarrow 1 - 12(\chi/\pi)^2$ with $\chi = \chi_R - \chi_L$.

If one edge is in $0 < \chi < \pi/2$ (Regime I or II) and the other edge is in $\pi/2 < \chi < \pi$ (Regime III or IV), then the singularity crossing modifies the c_{eff} formula. Especially when one edge is in Regime II ($0 < \chi < \pi/2$ and $0 < \eta < \pi/2$), and the other edge in Regime IV ($\pi/2 < \chi < \pi$ and $0 < \eta < \pi/2$), then c_{eff} is linearly decreasing in the scale r , which indicates the opposite sign of boundary terms excites the one-particle state of the same sign of boundary terms. Similar behavior is obtained for Ising model when opposite boundary magnetic fields are applied to both edges. The magnetic field should not be too strong ($-1 < k < 0$), otherwise the opposite fields spoil the field theory and result in the complex free energy.

In ND-type, ($m_B^{(L)} < 1\sqrt{2}$ and $m_B^{(R)} > 1\sqrt{2}$), still UV limit and massless limit have their own domain. In the extreme limit ($m_B^{(L)} \rightarrow 0$ and $m_B^{(R)} \gg 1$), one may see that UV limit is the compact bosonic CFT with $c_{\text{eff}} \rightarrow 1 - 12(\alpha/\pi)^2$. On the other hand, the massless limit gives $c_{\text{eff}} \rightarrow -1/2$.

The similar singularity effect on RG flow is expected to be persistent when bsG goes beyond free Fermi limit. However, the presence of more species of particles and boundary bound states makes RG flow more complicated and the numerical analysis will be more difficult due to the numerical instability.

It is noted that the singularity analysis for the case of opposite boundary terms will be useful to study other boundary field theories. In Ising model, the magnitude of opposite boundary fields is limited since the field theory breaks down. This does not happen

in bsG. On the other hand, in boundary affine Toda field theory, the boundary actions are given in 3 kinds only. Among them the (-)boundary action is not well understood [22, 23, 24]. It seems that the complete understanding of the boundary action requires the proper study of the singularity structure at the presence of (-)boundary action condition.

Acknowledgement

The author thanks Z. Bajnok, P. Dorey, R. Nepomechie, F. Ravanini and R. Tateo for valuable discussions, T. J. Lee for the work at the initial stage, and APCTP topical program during which this work initiated. This work is supported in part by Korea Research Foundation 2002-070-C00025.

Appendix

Ising model's reflection amplitude is given as

$$R_k(\theta) = i \tanh\left(\frac{i\pi}{4} - \frac{\theta}{2}\right) \frac{k - i \sinh \theta}{k - i \sinh \theta} \quad (7-1)$$

where $k = 1 - h^2$ with h the boundary magnetic field. (Note that h^2 is scaled by $2M$ where M the particle mass so that h is a dimensionless number.) Thus

$$K(\theta) = i \tanh\left(\frac{\theta}{2}\right) \frac{k + \cosh \theta}{k - \cosh \theta} \quad (7-2)$$

and the fugacity becomes

$$\lambda = \overline{K_L} K_R = \tanh^2\left(\frac{\theta}{2}\right) \frac{k_L + \cosh \theta}{k_L - \cosh \theta} \frac{k_R + \cosh \theta}{k_R - \cosh \theta}. \quad (7-3)$$

The effective central charge is given as [21]

$$c_{\text{eff}} = \frac{6r}{\pi^2} \int_{-\infty}^{\infty} d\theta \cosh \theta \log Z_{\text{Ising}}(\theta) \equiv c - 24\Delta, \quad (7-4)$$

where $\epsilon = 2r \cosh \theta$ with $r = RM$. $Z_{\text{Ising}}(\theta) = (1 + \lambda(\theta) e^{-\epsilon(\theta)})$ satisfies the periodicity, $Z_{\text{Ising}}(\theta + i2\pi) = Z_{\text{Ising}}(\theta)$ and $Z_{\text{Ising}}(\theta + i\pi) = Z_{\text{Ising}}(\theta) e^{\epsilon_0(\theta)}/\lambda_0(\theta)$.

According to singularity structure, the domain of parameters are classified into three regimes: $0 < k < 1$, $-1 < k < 1$ and $k < -1$. In each regime, the magnetic field h and $-h$ is to be distinguished. In fact, $h = 0$ (or $k = 1$) is the singular point in the parameter space h since one of $Z_0 S$ lies at real rapidity axis. The domains $h > 0$ and $h < 0$ are connected through the branch singularity. Thus two domains are not equivalent due to the existence of crossing singularities.

Regime $0 < k < 1$ is the weak magnetic field regime ($0 < h^2 < 1$) similar to the N-type in the text. There is a boundary bound state, which makes a pair of $Z_{\infty} CS$ at $\pm i\xi$ where $0 < \xi < \pi/2$ and $\cos \xi = k$. A pair of $Z_0 CS$ at $\pm i\theta_N$ with $0 < \theta_N < \xi$ is

squeezed between the pair of $Z_\infty CS$. c_{eff} is modified when the boundary magnetic fields are of opposite sign ($h_L h_R < 0$),

$$c_{\text{eff}} = -\frac{24r}{\pi} \left(\sin \theta_N - \sin \xi \right) + \frac{6r}{\pi^2} \oint_{-\infty}^{\infty} d\theta e^\theta \log Z_{\text{Ising}}(\theta). \quad (7-5)$$

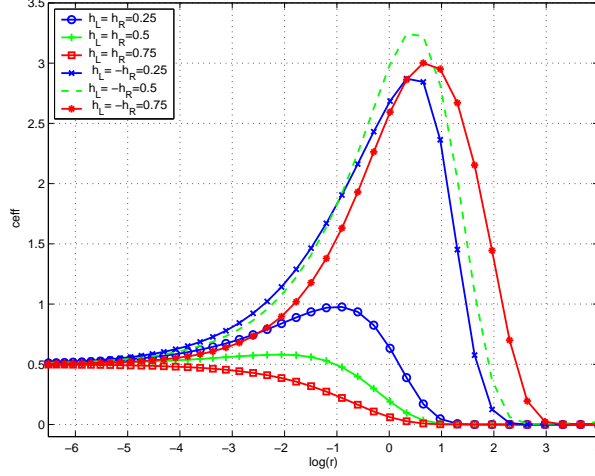


Figure 17: c_{eff} v.s. $\log(r)$ for $0 < k < 1$ (weak boundary magnetic field).

In regime $-1 < k < 0$ (boundary magnetic field $1 < h^2 < 2$), there is no boundary bound state. Nevertheless, $Z_\infty CS$ exists at $\pm i(\xi + \pi/2)$ ($0 < \xi < \pi/2$), outside of the physical strip. All $Z_0 CS$ lie at $\text{Im}(\theta) = \pi/2$ and $Z_0 CS$ is given as $\pm(\theta_D \pm i\pi/2)$. When the boundary magnetic fields are of opposite sign,

$$c_{\text{eff}} = -\frac{24r}{\pi} \left(\cosh \theta_D - \cos \xi \right) + \frac{6r}{\pi^2} \oint_{-\infty}^{\infty} d\theta e^\theta \log Z_{\text{Ising}}(\theta). \quad (7-6)$$

In figure 18 c_{eff} with $h_L h_R > 0$ is plotted. The case with $h_L h_R < 0$ is contrasted with that of same sign in figure 19 where the curves with the same sign are nearly overlapped and are not distinguished each other. In all cases, there is no resonance.

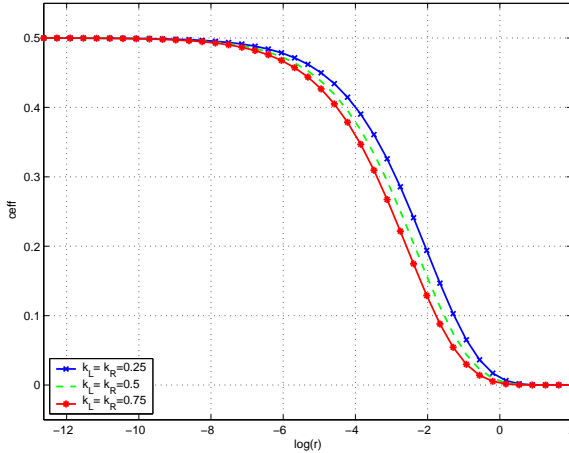


Figure 18: c_{eff} v.s. $\log(r)$ with $-1 < k < 0$. Boundary magnetic field of both edges are with same sign.

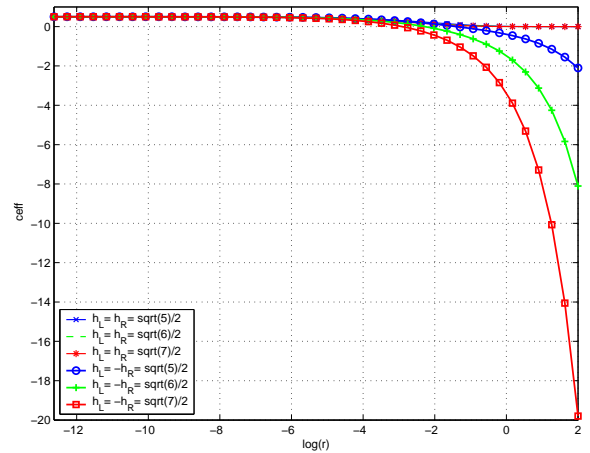


Figure 19: c_{eff} v.s. $\log(r)$ with $-1 < k < 0$. Boundary magnetic field of both edges are with opposite sign

Note that in figure 19, c_{eff} decreases linearly in r as $r \gg 1$ and when opposite boundary fields are given. (At IR limit, $\theta_D = 0$ and the integrated part vanishes in (7-6) so that the linear coefficient is proportional to $(1 - \cos \xi)$.) This trend of linearity is clearly seen in figure 20.

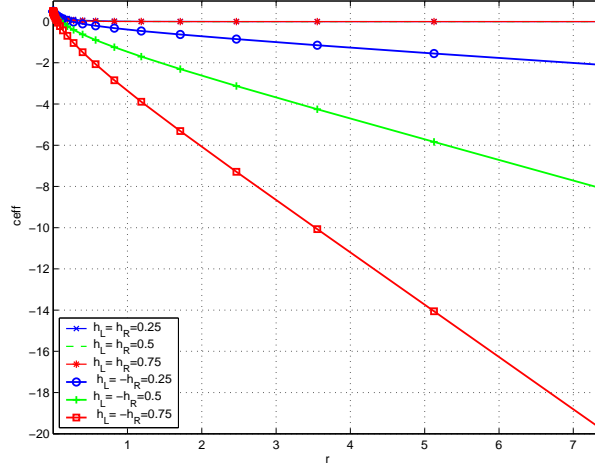


Figure 20: c_{eff} v.s. r for $-1 < k < 0$.

The linearity of c_{eff} in the Regime $-1 < k < 0$ shows the similarity to D-type of bsG. However, unlike bsG the plateau does not appear in this Regime but in Regime $k < -1$ (boundary magnetic field $h^2 > 2$). As given in figure 21, the stronger the boundary field becomes, the wider appears the plateau region which is identified as the massless limit. The massless limit is distinguished from the UV limit even though $c_{\text{eff}} \rightarrow 1/2$ in both limits. When $k > -1$, the massless limit coincides with the UV limit.

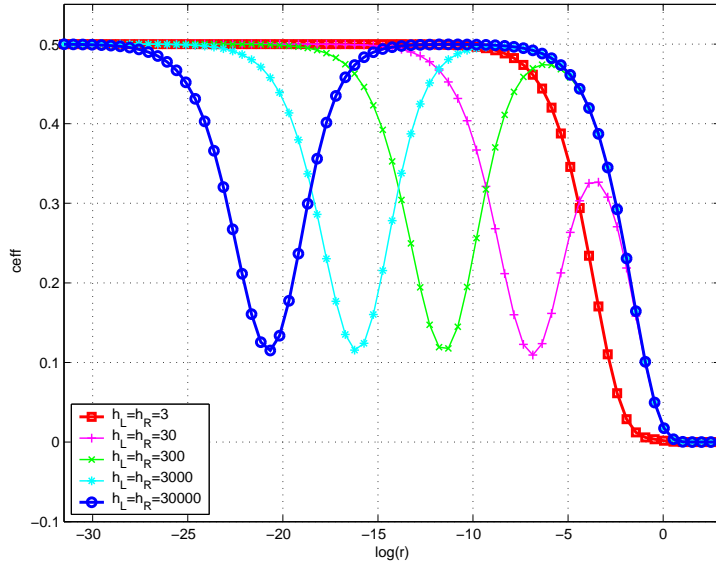


Figure 21: c_{eff} v.s. $\log(r)$ for $k < -1$.

When $k < -1$, the opposite boundary magnetic field makes the field theory unstable. The breakdown is due to $Z_\infty CS$ at $\pm(\xi \pm i\pi)$, where $\cosh \xi = |k|$ with real $\xi > 0$.

The singularity lies outside of the physical strip and becomes ‘resonant poles’. This crossing singularities result in a complex-valued c_{eff} and thus, free energy density becomes complex valued :

$$c_{\text{eff}} = -\frac{24r}{\pi} \left(\cosh \theta_D + i \sinh \xi \right) + \frac{6r}{\pi^2} \int_{-\infty}^{\infty} d\theta e^{\theta} \log Z_{\text{Ising}}(\theta), \quad (7-7)$$

where Z_0CS is at $\pm(\theta_D \pm i\pi/2)$.

Finally, if one edge is given with a vanishing boundary magnetic field $k \rightarrow 1$ and the other edge with a strong one $k \rightarrow -\infty$, the plateau appears corresponding to CFT limit of the mixed boundary condition, whose $c_{\text{eff}} = -1$ and the ground state has the conformal dimension $1/16$. (See figure 22.)

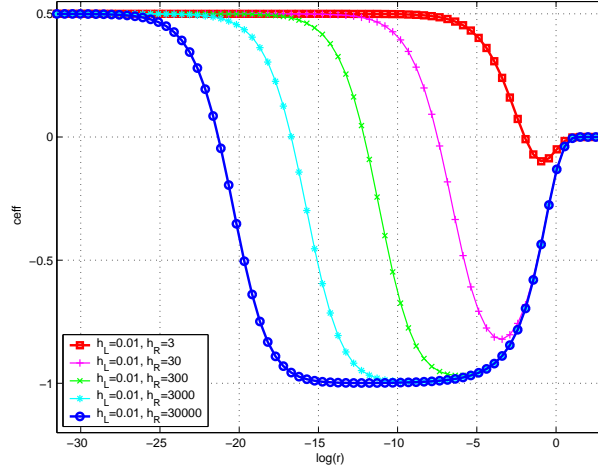


Figure 22: c_{eff} v.s. $\log(r)$. A weak (strong) boundary field is given at one (the other) edge.

References

- [1] A. B. Zamolodchikov, Int. J. Mod. Phys. **A4** (1989) 4235.
- [2] Al. B. Zamolodchikov, Nucl. Phys. **B342** (1990) 695.
- [3] C. N. Yang and C. P. Yang, J. Math. Phys. **10** (1969) 1115.
- [4] Al. B. Zamolodchikov, Nucl. Phys. **B358** (1991) 524.
- [5] T. R. Klassen and E. Melzer, Nucl. Phys. **B400** (1993) 547.
- [6] F. Ravanini, R. Tateo, A. Valleriani, Int. J. Mod. Phys. **A8** (1993) 1707.
- [7] P. A. Pearce, L. Chim, C. Ahn, Nucl. Phys. **B601** (2001) 539; **B660** (2003) 579.
- [8] C. Ahn, C. Kim, C. Rim and Al. B. Zamolodchikov, Phys. Lett. **B 541** (2002) 94.
- [9] S. Ghoshal and A. B. Zamolodchikov, Int. J. Mod. Phys. **A9** (1994) 3841 (Erratum-ibid **A9** (1994) 4353; S. Ghoshal, Int. J. Mod. Phys. **A9** (1994) 4801.

- [10] P. Dorey and R. Tateo, Nucl. Phys. **B482** (1996) 639; Nucl. Phys. **B515** (1998) 575.
- [11] J.-S. Caux, H. Saleur and F. Siano, Phys. Rev. Lett. **88** (2002) 106402.
- [12] T. Lee and C. Rim, Nucl. Phys. **B672** (2003) 487.
- [13] J.-S. Caux, H. Saleur and F. Siano, Nucl. Phys. **B672** (2003).
- [14] A. LeClair, G. Mussardo, H. Saleur and S. Skorik, Nucl. Phys. **B453** (1995) 581.
- [15] C. Ahn and R. Nepomechie, Nucl. Phys. **B676** (2004) 637.
- [16] M. Ameduri, R. Konik, A. LeClair, Phys. Lett. **B354** (1995) 376.
- [17] S. Mandelstam, Phys. Rev. D **11** (1975) 3026.
- [18] Al. Zamolodchikov in 5th Bologna Workshop (2001). on CFT and Integrable Models, September 26-29, 2001; Z. Bajnok, L. Palla and G. Takács, Nucl. Phys. **B622** (2002) 565.
- [19] H. Saleur, S. Skorik, N. P. Warner, Nucl. Phys. **B441** (1995) 421.
- [20] S. Skorik and H. Saleur, J. Phys. **A28** (1995) 6605; P. Mattison and P. Dorey, J. Phy. **A33** (2000) 9065; Z. Bajnok, L. Palla and G. Takács, Nucl. Phys. **B622** (2002) 548.
- [21] R. Chatterjee, Nucl. Phys. **B468** (1996) 439.
- [22] E. Corrigan, P. Dorey, R. Rietdijk, and R. Sasaki, Phys. Lett. **B333** (1994) 83-91.
- [23] V. Fateev, “Normalization Factors, Reflection Amplitudes and Integrable Systems”, **hep-th/0103014**; Mod. Phys. Lett. **A16** (2001) 1201; V. A. Fateev and E. Onofri, Nucl. Phys. **B634** (2002) 546.
- [24] C. Ahn, C. Kim, C. Rim, Nucl. Phys. **B628** (2002) 486.